Journal Pre-proofs

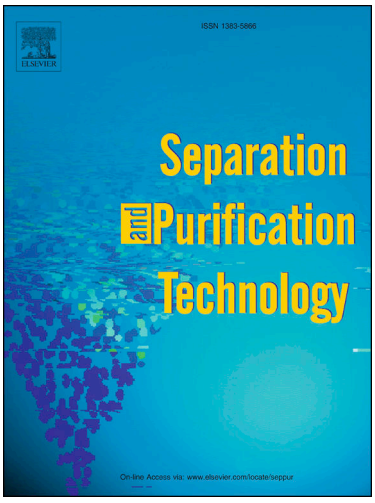

PSA Purification of waste hydrogen from ammonia plants to fuel cell grade

María Yá ñez, Frederico Relvas, Alfredo Ortiz, Daniel Gorri, Adélio Mendes, Inmaculada Ortiz

PII: S1383-5866(19)33150-8
DOI: https://doi.org/10.1016/j.seppur.2019.116334
Reference: SEPPUR 116334

To appear in: *Separation and Purification Technology*

Received Date: 19 July 2019
Revised Date: 6 November 2019
Accepted Date: 18 November 2019

Please cite this article as: M. Yá ñez, F. Relvas, A. Ortiz, D. Gorri, A. Mendes, I. Ortiz, PSA Purification of waste hydrogen from ammonia plants to fuel cell grade, *Separation and Purification Technology* (2019), doi: https://doi.org/10.1016/j.seppur.2019.116334

PSA PURIFICATION OF WASTE HYDROGEN FROM AMMONIA PLANTS TO FUEL CELL GRADE

María Yáñez[1], Frederico Relvas[2], Alfredo Ortiz[1], Daniel Gorri[1], Adélio Mendes[2,*] and Inmaculada Ortiz[1]

[1] Chemical and Biomolecular Engineering Department, ETSIIyT, University of Cantabria, Av. los Castros s/n, 39005, Santander, Spain.

[2] LEPABE - Laboratory for Process Engineering, Environment, Biotechnology and Energy, Faculty of Engineering, University of Porto, Rua Dr. Roberto Frias, 4200-465 Porto, Portugal

Tel.: +34 942201585; Fax: +34 942201591; *contact e-mail: mendes@fe.up.pt

*To whom correspondence should be addressed.

To be submitted to *Separation and Purification Technology*

July 2019

ABSTRACT

Industrial hydrogen-rich waste streams hold promises in their upgrading to feed fuel cell stacks. As in the ammonia synthesis process, a stream of up to 180–240 Nm^3 per ton of ammonia is purged to keep the inert gases concentration below a threshold value; this stream contains large hydrogen quantities, which could be recovered. In the current work, a four-column PSA unit has been used to produce a high-purity hydrogen stream for fuel cell applications from a synthetic mixture with a molar composition of 58 % H_2, 25 % N_2, 15 % CH_4 and 2 % Ar, based on ammonia purge gas. Firstly, a comparative performance of four commercially adsorbents was accomplished to obtain the adsorption isotherms of H_2, N_2, CH_4, and Ar, leading to the selection of 5A zeolite adsorbent. Then, the dynamic behavior of a packed bed was studied by single and multicomponent breakthrough experiments and simulated using Aspen Adsorption®. The results, simulations and experimental, indicate that after H_2 the first impurity to break thought the column is Ar, followed by N_2 and finally by CH_4. Then, a design-of-experiments (DoE) methodology was used to select the best operating conditions of the experimental cyclic PSA unit to reach different target hydrogen product concentrations; the overall PSA performance was evaluated in terms of purity and recovery of H_2 product. According to the results, the four-column PSA unit running at 9 bar produced a stream with and hydrogen concentration of 99.25 % and 99.97 % of H_2, with a recovery of 55.5 % and 75.3 %, respectively, and it mostly contained Ar and N_2 as impurities. In addition to the technical performance, the economic assessment concluded that the cost to compress, transport and purify waste hydrogen to a concentration of 99.97 % using a small-scale PSA unit from ammonia plants has been estimated in the range of 1.17 to 1.39 € kg H_2^{-1}, depending on the dispensing pressure of 350 or 700 bar, respectively. These assessments offer a cost-effective solution to produce high-purity H_2 as low cost transportation, allowing hydrogen penetration into the mass markets.

KEYWORDS

Hydrogen purification, ammonia purge gas, pressure swing adsorption (PSA), Zeolite 5A, adsorption equilibrium isotherms

1. INTRODUCTION

Interest in hydrogen, as a unique and versatile energy carrier, has been growing over the past decade as a way of enabling a full large-scale integration of renewables, in response to decarbonize all sectors of the economy and concerns about the global proved fossil-fuel reserves [1]. Energy production and use is the largest source of global greenhouse-gas (GHG) emissions , where transportation is a major contributor to climate change, emitting 32 % of CO_2 emissions in the European Union (EU) [2]. To meet world's agreed climate target defined under the Paris Agreement, worldwide stakeholders must pursue limit energy-related CO_2 emissions to less than 770 megatons per year by 2050 to preserve local air quality [3]. Hence, hydrogen-based energy storage systems will lead the way for the transition to a decarbonized energy system due to its significant potential for carbon neutrality along the entire hydrogen value chain.

Therefore, hydrogen demand for fuel cell applications is expected to grow rapidly in all sectors of the economy: transportation, buildings and industry. In this regard, hydrogen as a transportation fuel produced at a cost around 1.5 - 3 € kg^{-1} could be competitive with conventional fuels within the automotive industry, allowing hydrogen penetration into the mass markets. According to the European's 2030 vision, these prices would be viable by a diversity of clean production routes such as the conventional central steam-reforming of natural gas (SMR) combined with carbon capture and storage (CCS), and decentralized water electrolysis connected to wind or solar farms [4]. On the other hand, hydrogen sales price to mobility end-users is currently set at 9 - 10 € kg^{-1}, within the hydrogen refueling stations (HRS) in Europe. Nevertheless, EU-targets of hydrogen sales price assessed at nozzle by 2030 should be in the range of 4 - 6 € kg^{-1} to achieve cost parity with conventional fuels; but even these figures strongly depend on natural gas and electricity prices to achieve profitability [5,6].

Among the fuel cell technologies, polymer electrolyte membrane fuel cells (PEMFC) are one of the most promising electrochemical devices that when fed with hydrogen produce electricity in a very efficient and clean way. The advantages of PEMFC devices, such as rapid start-up, high electrical efficiency, silence, low pollutant emissions and ease of installation, motivate their application to portable, transportation and stationary end-uses [7]. High-purity hydrogen is beneficial to achieve lifetime EU-targets of fuel cell systems by 2030 (28,000 h) to become a competitive alternative to conventional internal combustion engines (ICE) [8].

Besides, hydrogen fuel index should comply with ISO 14687 standards, which are divided in three parts: Part 1 - for all types of applications, except those including PEMFCs; Part 2 - for road vehicle application, and Part 3 - for stationary application. According to these standards, hydrogen fuel index of 98% is required to feed ICEs (ISO 14687-1), of 99.9 % for PEMFC stationary appliance systems (ISO 14687-3), and of 99.97 % for PEMFC road vehicle systems (ISO 14687-2) [9–11].

At the same time, H_2-rich industrial waste streams are considered potential and promising sources for hydrogen [12,13]. The hydrogen from these waste streams, which are normally burned or dumped to the atmosphere, can potentially be recovered and used as feedstock for the manufacture of commodities such as ammonia or methanol, or even upgraded to fuel for both transportation and stationary applications. In a previous work [14], we have reinforced the fact that the use of inexpensive surplus hydrogen sources offers an economic approach to cover hydrogen demand in the very early stage of transition to the future global hydrogen-incorporated economy. Depending on the industrial origin, low-quality H_2 streams could contain different types of contaminants such as H_2O, H_2S, CO_2, C_2^+, CH_4, CO and N_2, that can affect performance and durability of the fuel cells in different ways, permanently or reversibly [15].

Developments in hydrogen separation processes are driven not only by cost and performance, but also by the purity requirements of the final application [16]. Particularly, stand-alone pressure swing adsorption (PSA) technology has a number of attractive characteristics, such as low energy requirements and low capital investment costs to produce high-purity products [17,18]. Industrial PSA units typically comprise a set of columns packed with an adsorbent, which operate simultaneously in an adsorption/regeneration cycle, in such a way that each bed undergoes the same sequence of elementary steps, but at different times. PSA process can produce H_2 with purities between 98 % and +99.99 %, with 70 - 90 % H_2 recovery in large units with more than 12 columns and operation pressures above 20 bar [19]. Regarding the mechanism, most of the PSA processes are equilibrium driven where the selectivity depends on differences in the equilibrium affinities [20]. The adsorption step is carried out at high pressure to retain all impurities; whereas the regeneration step is performed by reducing the total pressure of the bed. Therefore, the purified H_2 breaks through the column at near feed pressure, whereas the tail gas is at very low pressure to maximize H_2 recovery. This operating mode eliminates compression steps afterwards, and therefore permits to reduce energy consumption.

Intensive research has been carried out to improve the performance of the PSA process, either in terms of H_2 recovery or in unit size, focused on a variety of industrial effluents, such as SMR off gas [21], refinery off gases [22], coke oven gas [23,24] and coal gas [25]. The key development goals of PSA are to increase the yield of the units and to reduce the costs of smaller PSA systems [16]. With a growing demand of distributed hydrogen production, the challenge in H_2 purification becomes more evident at small-scale PSA units, in which lower recovery values are found, *ca*. <70 %, due to the lower operating pressure also used that gives less flexibility for cycle optimization [26].

In the ammonia synthesis process, a stream of up to 180–240 Nm^3 per ton of ammonia is purged to keep the inert gases concentration below a threshold value; this stream contains large hydrogen quantities, which could be recovered. The molar composition range of the cleaned purge gas, after water scrubbing, is: 54-67 % H_2, 18-25 % N_2, 8-15 % CH_4, 2-6 % Ar, less than 2500 ppm NH_3 and small traces of krypton and xenon [27,28]. In more recent designs, this hydrogen is mostly recovered and recycled to the synthesis loop via membrane contactors or cryogenic systems, but some part of the cleaned purge gas is usually added to the reformer fuel, or even directly released to the atmosphere [29,30].

A significant research effort has been already undertaken to upgrade this waste gas stream, which contains impurities, and improve hydrogen end-use. In 1998, Soon-Haeng Cho et al. reported a two-stage PSA process packed with zeolite 13X for argon and hydrogen recovery, simultaneously [31]. Although that study obtained high-hydrogen purity (> 99 %) in a pilot-plant PSA, there is a lack of information regarding H_2 recovery and the impurity content of the light product stream. Among other purification technologies under study, a catalytic Pd–Ag membrane reactor to produce pure hydrogen from ammonia purge gases has been reported by Rahimpour et al. [32,33]. Recently, a different research work evaluated the integrated configuration of the catalytic H_2-permselective membrane reactor and a solid oxide fuel cell for the flare and purge gas recovery from ammonia plants [34]. To our knowledge, no study has yielded significant results in terms of performance as well as cost for upgrading H_2 via four-column PSA unit using purge gases from ammonia industry.

The overall goal of this work was to evaluate experimentally a four-bed PSA process for purifying H_2-containing gas by using a four-component hydrogen mixture as a simulated ammonia synthesis vent gas (hereinafter called ammonia purge gas (APG)), described in Table 1.

Table 1. Case study ammonia purge gas (APG) parameters [35–37]

Specifications	Value
Purge gas flow rate (Nm^3 ton^{-1} NH_3)	180 - 240
Purge gas pressure (bar)	150 - 200
Temperature (°C)	*ca.* 20
Gas composition (% vol.)	-
H_2	58.0
N_2	25.0
CH_4	15.0
Ar	2.0

The adsorption equilibrium isotherms of H_2, N_2, CH_4, and Ar on several commercially adsorbents are obtained and, the most suitable adsorbent was selected and further characterized. Then, the adsorptive properties of the selected adsorbent were confirmed by single and multicomponent breakthrough runs and simulations. Once the breakthrough times were obtained for a single column, a design-of-experiments (DoE) was conducted to optimize the lab four-column PSA unit to produce target hydrogen purities at maximum recoveries. In addition to the technical performance, a brief economic analysis is provided for the hydrogen purification.

2. MATERIALS AND METHODS

2.1. Materials

For accomplishing the hydrogen purification, a set of four commercial adsorbents was selected and the corresponding properties are presented in Table 2. These adsorbents are an activated carbon (2GA-H2, Kuraray CO., Ltd., Japan) and zeolites LiX (ZEOX Z12-07, Zeochem AG, Switzerland), 13X (13XBFK, CWK-Chemiewerk Bad Köstritz, Germany) and 5A (5ABFK, CWK).

Table 2. Physical properties of the studied adsorbents

Adsorbent	Type	Cation	Structure	d_p (mm)	ρ_p (g cm^{-3})
AC	Pellet	-	Amorphous	1.2	2.1±0.1
13X	Spherical	Na^+	X	1.6-2.5	2.3±0.1
5A			A	1.6-2.5	2.3±0.1
LiX		Li^+	X	0.4-0.8	2.4±0.1

Prior to the isotherm measurements, zeolites were regenerated at 375 °C overnight under synthetic air flow. After regeneration, the temperature was allowed to decrease slowly at 1 °C min^{-1}. Helium pycnometry was performed to determine the structural volume of the samples and then the density of the adsorbents. For the multicomponent breakthrough experiments, a tank was used to prepare the synthetic gas mixture under study. All gases in this study had purities higher than 99.99 % and were supplied by Linde.

2.2. Methods

2.2.1. Equilibrium isotherms

Single-component adsorption isotherms were obtained using the volumetric method, described elsewhere [38], for H_2, N_2, CH_4 and Ar at different temperatures (20 °C, 40 °C and 60 °C) and pressure up to 7 bar. By a mass balance, assuming ideal gas behavior and knowing the pressure decay inside the sample vessel, which initially has been evacuated to P < 0.01 mbar, it is possible to determine the amount of adsorbed gas. In this work, adsorption equilibrium isotherms were fitted to the dual site Langmuir (DSL) equation, according to Eq. (1) [39].

$$q_{\mathrm{i}}^{*} = \frac{q_{\mathrm{max},1} \cdot b_1 \cdot P_{\mathrm{i}}}{1 + b_1 \cdot P_{\mathrm{i}}} + \frac{q_{\mathrm{max},2} \cdot b_2 \cdot P_{\mathrm{i}}}{1 + b_2 \cdot P_{\mathrm{i}}} \qquad \text{Eq. (1)}$$

where q_{i}^{*} is the molar concentration in the adsorbed phase (mol kg^{-1}), $q_{\mathrm{max},1}$ and $q_{\mathrm{max},2}$ are the maximum adsorbed concentration on sites 1 and 2, respectively (mol kg^{-1}); P_{i} is the partial pressure in the gas phase (bar); and b_1 and b_2 are the affinity constants for site 1 and 2, respectively (bar^{-1}). Obtaining the adsorption isotherms at three different temperatures, T_1 to T_3, allows determining the heats of adsorption using Eq. (2) – (3), where b_∞ is the pre-exponential factor of the affinity constant and *R* is the gas constant. For the breakthrough simulations which are further described below, it was assumed that the heats of adsorption on the first and second sites are equal ($\Delta H_1 = \Delta H_2$).

$$b_1 = b_{\infty,1} \cdot \mathrm{e}^{\Delta H_1 / \mathrm{R}T} \qquad \text{Eq. (2)}$$

$$b_2 = b_{\infty,2} \cdot \mathrm{e}^{\Delta H_2 / \mathrm{R}T} \qquad \text{Eq. (3)}$$

Thus, parameters $q_{\mathrm{max},1}$, $q_{\mathrm{max},2}$, $b_{\infty,1}$, $b_{\infty,2}$, ΔH were calculated by a non-linear data fitting of the experimental adsorption isotherms, minimizing the residual sum of squares, RSS, as follows:

$$RSS\ (\%) = \sum_{T=T_1}^{T_3} \sum_{k=1}^{N} \left(q_{\mathrm{i,exp}}^{*} - q_{\mathrm{i,mod}}^{*} \right)^2 \qquad \text{Eq. (4)}$$

with $q_{\mathrm{i,exp}}^{*}$ and $q_{\mathrm{i,mod}}^{*}$ as the experimental and estimated adsorbed concentration, respectively; k is the number of data points per experimental isotherm and gas component; and N is total number of experimental points.

The equilibrium separation factor $\alpha_{i/j}$ was used to assess the adsorbent ability to separate the gases under study, which is usually expressed using Eq. (5) [40,41]:

$$\alpha_{i/j} = \frac{q_i^*/q_j^*}{P_i/P_j} \quad \text{Eq. (5)}$$

where q_i^* and q_i^* are the molar loading of species *i* and *j* at partial pressure of P_i and P_j, respectively, under the process conditions. Therefore, separation factor in equilibrium-based separation processes indicates the effectiveness of the separation performance between gases *i* and *j* by the considered adsorbent, and therefore they are discussed in the following section.

2.2.2. Adsorption breakthroughs

2.2.2.1. Experimental set-up

A set of breakthrough experiments was carried out in a fixed-bed column for the selected 5A zeolite adsorbent, recording the history of the outlet stream composition – breakthrough curves. From the breakthrough curves, the amount of gas adsorbed can be evaluated allowing to validate the adsorption equilibrium isotherms. Moreover, one can evaluate the duration of the adsorption step in the PSA cycle [42].

Single and multicomponent breakthrough experiments were conducted in an experimental set-up as described elsewhere [43] and schematically pictured in Figure 1. The lab set-up is placed in a thermostatic chamber to ensure isothermal operation, where the packed column with the selected adsorbent is equipped with two thermocouples and two pressure transducers at the entrance and the exit of the column; the process pressure is handled using a high precision backpressure regulator (Equilibar EB1LF2). The feed flow rate is controlled using Bronkhorst mass flow controllers' series F-201C (0−0.1 $L_N\,min^{-1}$), F-112CV (0−1 $L_N\,min^{-1}$) and F-201CV (0−10 $L_N\,min^{-1}$), and a mass flow meter series F-111C (0−3 $L_N\,min^{-1}$) for measuring the exit flowrate. The composition of the outlet gas is determined using a mass spectrometer (Pfeiffer GSD 301 O2). The characteristics of the column and the experimental conditions are detailed in Table 3.

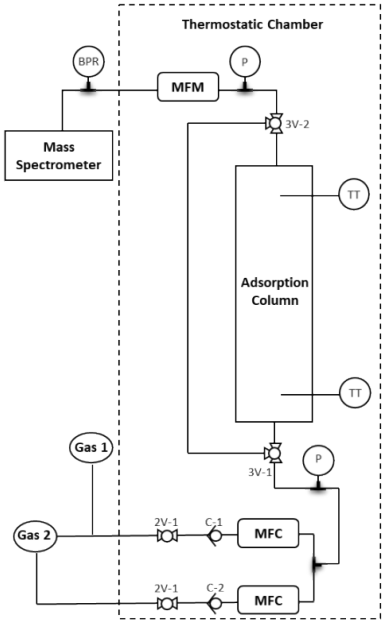

Figure 1. Single adsorption column flow diagram. MFC, flow controller; MFM, flow meter; 2V, 2-way valve; 3V, 3-way valve; C, check valve; TT, thermocouple; P, pressure transducer; BPR, back pressure regulator.

Adsorption and desorption breakthrough measurements were carried out at 40 °C, varying the pressure and feed flow rate. After each adsorption assay, desorption breakthroughs were performed passing pure He through the column. Owing to the available mass spectrometer could not operate with streams with a molar hydrogen concentration >20 %, the measurements were carried out using gas mixtures balanced with He.

Table 3. Characteristics of the column and experimental conditions

Column characteristics	**Value**
L_{bed} (cm)	33.8
d_{in} (cm)	3.16
d_0 (cm)	3.49
TT distance from top and bottom (cm)	2.5
Adsorbent type	5A zeolite
m_{ads}(g)	193.12
Feed conditions	**Value**
He:N_2	75:25
He:Ar	98:2
He:CH_4	85:15
He:H_2	80:20
He:H_2:N_2:Ar:CH4	38:20:25:2:15
Q_{F} (L_N min^{-1})	0.5 / 2.75
P (bar)	1 / 4.5
T (ºC)	40

2.2.2.2. Modeling and simulation of breakthrough curves

The breakthrough curves were simulated using Aspen Adsorption® V.10; the partial differential equations (PDEs) corresponding to mass, energy and momentum balances are discretized over an uniform grid using algebraic approximations with suitable boundary and initial conditions. The first order space derivative was approximated using an upwind differencing scheme (UDS) applied in 60 nodes. The resulting ordinary differential equations (ODEs) are further integrated in time. Accordingly, a non-isothermal and non-adiabatic model was applied using measured parameters (isotherm parameters, bed geometry, etc.) and other properties, for instance, heat capacity and conductivity, as input values found in the literature.

The main assumptions of the mathematical model used for simulating breakthrough curves are [42,44]:

- ideal gas behavior throughout the column.
- negligible radial gradients (P, T, y).
- non-isothermal and non-adiabatic conditions with gas and solid heat conduction.
- the adsorption rate is approximated by the linear driving force (LDF) model.
- convection with constant dispersion for all components through the bed based on the axial dispersed plug flow-model.
- adsorption equilibrium described by DSL isotherms, forcing the heat of adsorption of each site to be equal.
- pressure drop described by Ergun's equation.
- constant heat transfer coefficients.
- constant and homogeneous bed porosity along the bed length.

According to these assumptions, the governing equations and input values are fully explained in Appendix B. After that, the developed model was validated comparing selected simulation results with the corresponding breakthrough experiments.

2.2.3. Experimental PSA unit

2.2.3.1. Process description

A four-column PSA was optimized to produce hydrogen for fuel cells applications from a synthetic mixture based on purge gases from ammonia industry. A sketch of the PSA unit, described elsewhere [45], is shown in Figure 2. The PSA unit was packed with 5A zeolite and a fifth column was used as a tank to store part of the product needed for the

selected adsorption cycle. Additionally, two tanks were installed, one for minimizing pressure fluctuations and the other for collecting the light product. The packed columns were made of stainless steel with a length of 34.5 cm, an inner diameter of 2.7 cm, and a wall thickness of 0.15 cm. Three Bronkhorst mass flow meters' series F-112AC (0−20 L_N min^{-1}), F-111C (0−2 L_N min^{-1}), and F-111B (0−3 L_N min^{-1}) were used to measure the flow rate of the feed, purge and product streams, respectively. A needle valve was placed at the top of the columns to regulate the purge and backfill flowrates. A Bronkhorst pressure controller series P-702CV (0-10 bar) was placed after the product tank to maintain constant light product pressure. Four pressure transducers at the bottom of each bed were used to obtain the pressure history during operation. Check valves and solenoid valves were installed to direct the flow according to the PSA cycle and prevent reverse flow. The analysis of the cyclic steady state outlet gas composition was performed using an online gas chromatograph (Dani GC 1000 equipped with a TCD detector). N_2 and Ar concentration was measured as a whole. The detection limit in all cases, N_2 + Ar and CH_4 concentrations, were assumed to be <100 ppm. All instruments were connected to a computer using a data acquisition card (LabView interface); a routine written in the LabView platform was used for acquiring all data while a Visual Basic routine was used for controlling the solenoid valves according to the PSA cycle.

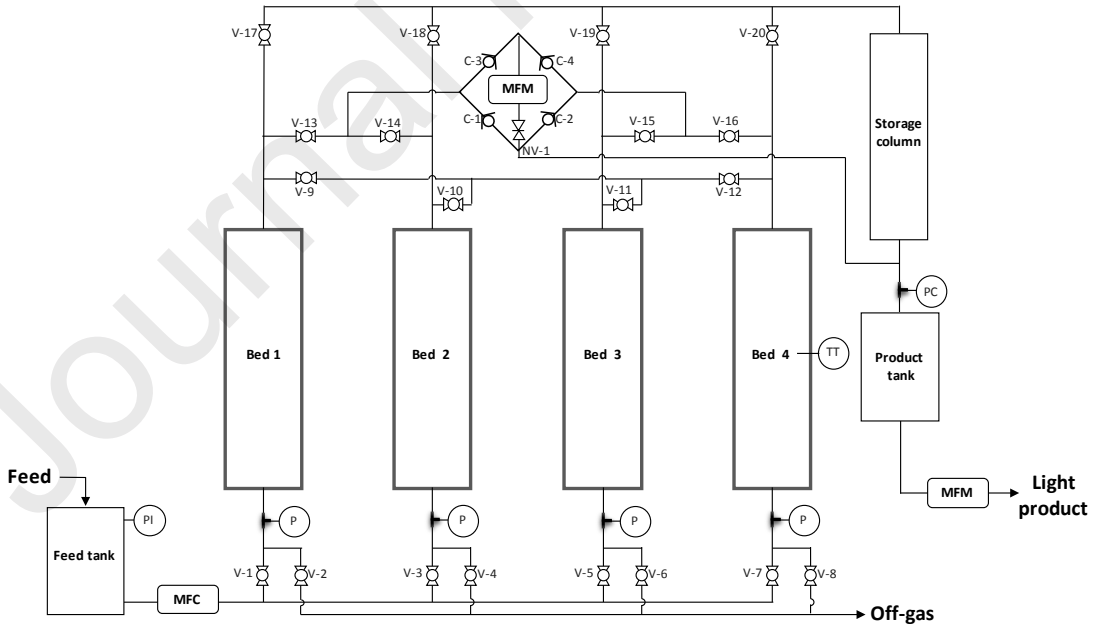

Figure 2. Schematic of the four-column PSA system. MFC, flow controller; MFM, flow meter; V, Solenoid vales; C, check valve; NV, Needle valve; TT, thermocouple; P, pressure transducer; PC, pressure controller.

During the PSA cycle, each column run 9 elementary steps with different durations resulting in a 12-events cycle as described (following *Bed 1*): I) adsorption (AD) at the high pressure, II) H_2 product is split in two parts (AD/BF); one part of the stream flows to the storage column and the other is conducted to pressurize (backfill) *Bed 2*, which is the next adsorption bed, III) depressurization pressure equalization (DPE) down to an average pressure between *Bed 1* and *Bed 3*, IV) blowdown (BD) to the low cycle pressure, V) purge with H_2 product (PG), VI) Idle (IDLE), VII) first pressurization pressure equalization (FPPE) up to an average pressure between *Bed 1* and *Bed 3*, VIII) backfill with H_2 product (BF) and IX) second pressurization pressure equalization (SPPE) with the effluent from the producing bed *Bed 4*. Before operation, the PSA was pressurized with H_2 at the adsorption high pressure.

Table 4. Sequence of 12-events PSA cycle [a]

Events	1	2	3	4	5	6	7	8	9	10	11	12
Bed 1	AD		AD/BF	DPE	BD	PG		IDLE		FPPE	BF	SPPE
Bed 2	FPPE	BF	SPPE	AD		AD/BF	DPE	BD	PG		IDLE	
Bed 3	PG	IDLE		FPPE	BF	SPPE	AD		AD/BF	DPE	BD	PG
Bed 4	DPE	BD	PG	IDLE			FPPE	BF	SPPE	AD		AD/BF

[a] Adsorption (AD), providing backfill (AD/BF), depressurization pressure equalization (DPE), blowdown (BD), purge (PP), idle (IDLE), first pressurization pressure equalization (FPPE), backfill (BF), second pressurization pressure equalization (SPPE).

The cyclic sequence for the process and a typical pressure history along the cycle are given in Table 4 and Figure 3, respectively. The longer cycle steps (AD, PG, IDLE, BF) have a duration of t_{ad}= 60-90 s, whereas the shorter cycle steps (AD/BF, DPE, BD, FPPE, SPPE) were fixed at t_{eq}= 4 s.

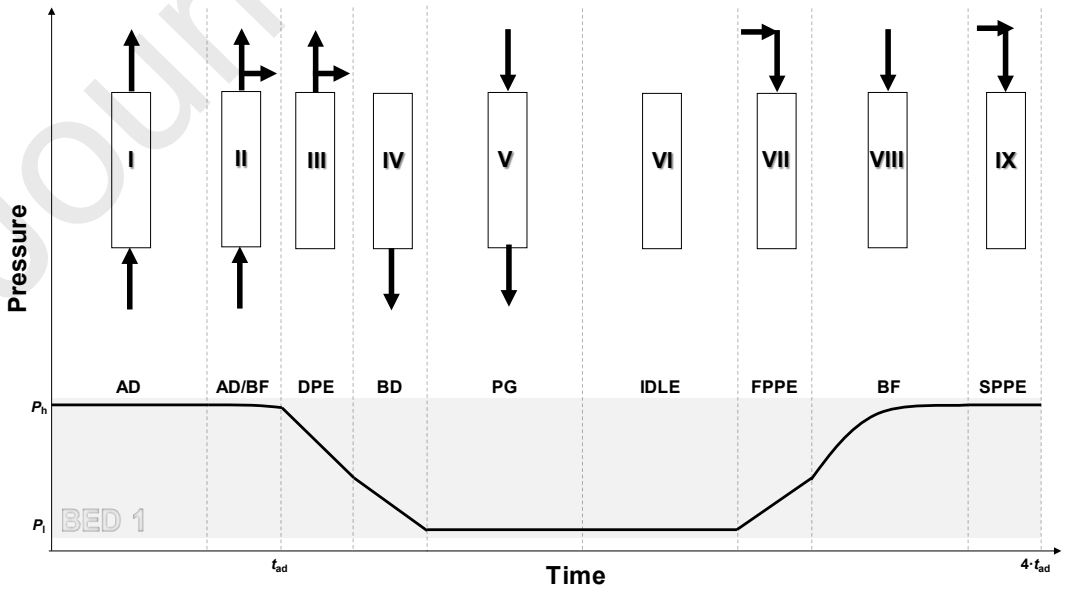

Figure 3. Schematic diagram of the cycle sequences used in the PSA experiments

2.2.3.2. Experimental design

In this study, 9-step 4-bed PSA experiments, described in Figure 3, were carried out under various operating conditions. The system performance depends on several process variables such as temperature of operation, cycle sequence, high and low operating pressures, purge-to-feed P/F ratio, etc.

Herein, P/F ratio; adsorption pressure, P_{h}; and adsorption time, t_{ad}, which includes time of elementary steps I and II, t_{ad}= $t_{\mathrm{I}} + t_{\mathrm{II}}$, were selected as three dimensionless factors. Other variables were preset at defined values, such as low operating pressure P_{l}= 1 bar; feed flow rate, Q_{F}= 2 L_N min^{-1} and equalization time, t_{eq}= 4 s. To compare performances among the PSA operations, the performance indicator parameters were assessed in terms of hydrogen purity, HP, as well as productivity and recovery, HR, defined as shown in the following Eq. (6) - Eq. (8) [39,46]:

$$HP = \frac{\int_0^{t_{\mathrm{ad}}} y_{\mathrm{prod,\,H_2}} \cdot Q_{\mathrm{prod}} dt}{\sum_{i=1}^{n} \int_0^{t_{\mathrm{ad}}} y_{\mathrm{prod,i}} \cdot Q_{\mathrm{prod}} dt} \cdot 100 \qquad \text{Eq. (6)}$$

$$HR = \frac{\int_0^{t_{\mathrm{ad}}} y_{\mathrm{prod,\,H_2}} \cdot Q_{\mathrm{prod}} dt}{\int_0^{t_{\mathrm{ad}}} y_{F,\,\mathrm{H_2}} \cdot Q_{\mathrm{F}} dt} \cdot 100 \qquad \text{Eq. (7)}$$

$$Productivity = \frac{\sum_{i=1}^{n} \int_0^{t_{\mathrm{ad}}} y_{\mathrm{prod,i}} \cdot Q_{\mathrm{prod}} dt}{m_{\mathrm{ads}} \cdot t_{\mathrm{cycle}}} \qquad \text{Eq. (8)}$$

The influence of the aforementioned factors on the system performance has been assessed and optimized following a DoE methodology [47]. This creates a factorial experimental plan by both reducing the number of experimental runs required and also maximizing the accuracy of the results obtained [48]. Response surface methodology (RSM) uses multiple regression analysis to relate predicted response with the independent factors [49]. RSM analysis was conducted using the statistical software JMP 7.0 (SAS Institute Inc.). In this work, it was used a central composite design (CCD) method for the factorial study that combines two-level three-factorial points, 2^3, plus 2x3 axial points, with two replicas at the center point, leading to a total number of sixteen experiments [50]. For generating design matrices, three dimensionless factors, X_{i}, for each independent factor, ranging from -1 to +1 as the lower and upper limits, have been coded according to:

$$X_1 = \frac{t_{\mathrm{ad}} - \bar{t}_{\mathrm{ad}}}{\frac{t_{\mathrm{ad,+1}} - t_{\mathrm{ad,-1}}}{2}}; \quad X_2 = \frac{P_{\mathrm{h}} - \overline{P}_{\mathrm{h}}}{\frac{P_{\mathrm{h,+1}} - P_{\mathrm{h,-1}}}{2}}; \quad X_3 = \frac{P/F - \overline{P/F}}{\frac{P/F_{+1} - P/F_{-1}}{2}} \qquad \text{Eq. (9)}$$

The experimental values were fitted to an empirical second-order polynomial equation, which describes the effect of the selected factors upon the process responses as represented in Eq. (10):

$$\hat{y}\,(HP;HR) = \beta_0 + \beta_1 X_1 + \beta_2 X_2 + \beta_3 X_3 + \beta_4 X_2 X_1 + \beta_5 X_1 X_3 + \beta_6 X_2 X_3 + \beta_7 {X_1}^2 + \beta_8 {X_2}^2 + \beta_9 {X_3}^2 \quad \text{Eq. (10)}$$

where $\hat{y}$ is the process response; X_1, X_2 and X_3 are the dimensionless process factors; and (β_0), (β_1, β_2, β_3), (β_4, β_5, β_6), and (β_7, β_8, β_9) represent the intercept, linear, interaction, and quadratic coefficients, respectively. The analysis of variance (ANOVA) of the data was performed to assess the fitness of the polynomial model. According to Eq. (10), optimization of the response $\hat{y}$ can be applied based on purity requirements for industrial use, road vehicle or stationary applications; meanwhile hydrogen recovery is maximized. Conforming to screening experiments and literature data, the ranges of the factors as well as the operating conditions of the PSA tests were selected and shown in Table 5.

Table 5. Operating conditions of the PSA runs

Column characteristics		**Value**
L_{bed} (cm)		35
d_{in} (cm)		2.7
d_0 (cm)		3.0
Thermocouple distance from top and bottom (cm)		15
Adsorbent type		5A zeolite
m_{ads} per column (g)		136.1 ± 0.7
Fixed conditions		**Value**
H_2:N_2:Ar:CH_4 (% vol.)		58:25:15:2
Q_{F} (L_N min^{-1})		2
P_{l} (bar)		1
T (ºC)		*ca.* 25
t_{eq} (s)		4
t_{cycle}(s)		$4 \cdot t_{\mathrm{ad}}$
Minimum number of PSA cycles		40
Variable conditions		
Symbol	**Lower bound**	**Upper bound**
P/F (-)	0.1	0.2
t_{ad} (s)	60	90
P_{h} (bar)	7	9

3. RESULTS AND DISCUSSION

3.1. Adsorption equilibria

Adsorption isotherms of H_2, N_2, CH_4, and Ar on the material adsorbents given in Table 2, for three temperatures (20 °C, 40 °C and 60 °C) and pressures up to 7 bar. Equilibrium adsorption data for all the candidate adsorbents under study is fully set out in Appendix A. To compare the performance of the adsorbents, equilibrium separation factors of H_2 over the other gases (H_2:N_2:CH_4:Ar, 58:25:15:2 %v/v) are summarized in Figure 4. According to Eq. (5), the separation factor depends on the relative equilibrium quantities of each adsorbed species under the process conditions. Therefore, the partial pressure of each gas was stated considering a pressure swing between high pressure, $P_h \sim 9$ bar, and the pressure, $P_l \sim 1$ bar, which were used during the PSA operation.

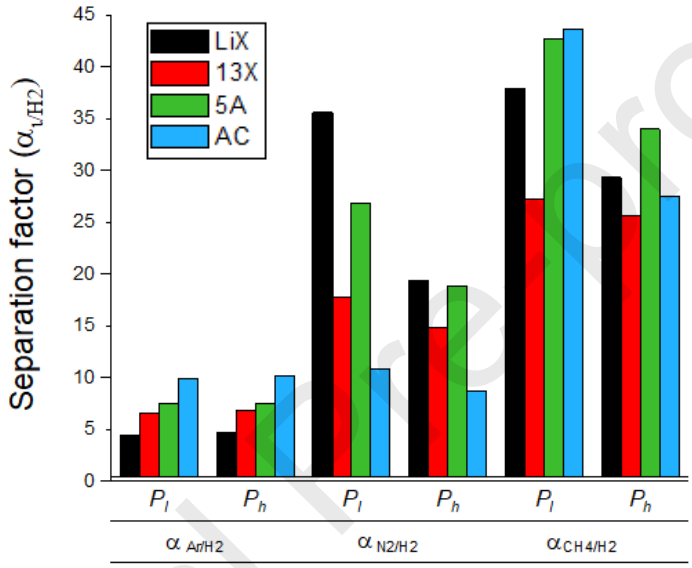

Figure 4. Separation factor between H_2 and the other gases i, at $\boldsymbol{P_h}$ and $\boldsymbol{P_l}$ pressures for different adsorbents; LiX (black), 13X (red), 5A (green) and AC (blue).

Figure 4 shows that the Ar/H_2 separation factor is the lowest for all adsorbents followed by N_2 and then CH_4. This means that Ar is a tricky gas to separate from H_2 without decreasing hydrogen recovery. Furthermore, zeolite LiX has the lowest Ar/H_2 separation factor, 4.6, followed by zeolites 13X, 6.7; 5A, 9.4, and the highest value is obtained by activated carbon AC, 10.2. On the contrary, LiX zeolite has the highest N_2/H_2 separation factor, 19-37, with a considerable difference between pressure swing values as it is expected looking at the isotherm curvature. This zeolite is followed by 5A zeolite, 16-21; 13X, 14-18 and AC, 8-11. Regarding CH_4/H_2 separation factor, the zeolite 5A accounts for the highest values, 43-56, followed by AC, 27-45, LiX, 29-39, and then 13X, 25-28. According to these results, activated carbon AC is the best adsorbent for Ar removal, whereas LiX and 5A zeolites perform better to remove N_2 and CH_4, respectively, from the feed. Therefore, 5A zeolite appears as the best choice for purifying H_2 from ammonia purge gas stream since it displays the best balance among all separation factors; besides

zeolite 5A is a robust cost-effective adsorbent. For that reason, this material was further characterized.

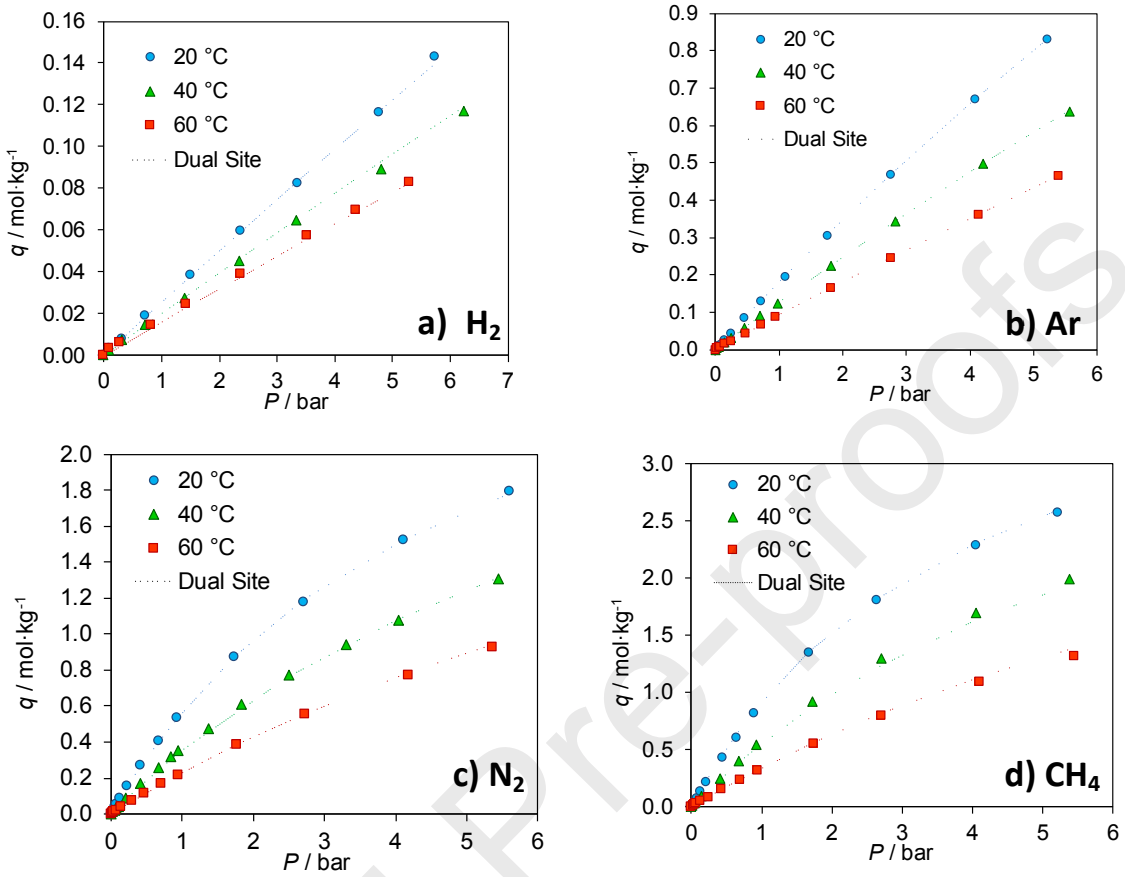

Figure 5. Adsorption isotherms on 5A zeolite for a) H_2, b) Ar, c) N_2 and d) CH_4 at 20 °C (blue); 40 °C (green); and 60 °C (red).

According to the adsorption isotherms plotted in Figure 5, the order of adsorption capacity on zeolite 5A up to 7 bar is H_2 << Ar < N_2 < CH_4. It is also observed that the adsorbed concentration increases with pressure with a linear trend for H_2 and Ar, and slightly favorable isotherms for N_2 and CH_4. On the contrary, the adsorption capacity decreases when the temperature increases due to the exothermic behavior, according to Eq. (1). As illustrated in Figure 5, dotted lines represent the DSL model, which is shown to suitably represent the experimental data. In the 5A zeolite, the adsorbed concentration of H_2 at 20 °C and 2 bar is 0.049 mol kg^{-1}, which is in agreement with similar studies in literature; i.e., ~ 0.036 mol kg^{-1} at 20 °C [51] and ~0.028 mol kg^{-1} at 25 °C [52]. Regarding the equilibrium adsorbed concentrations of the other adsorbates in the same conditions, Ar is 0.331 mol kg^{-1}, N_2 is 0.967 mol kg^{-1} and CH_4 is 1.503 mol kg^{-1}. For this material, relatively lower adsorbed concentrations have been reported in literature; i.e., for N_2, ~ 0.5-0.8 mol·kg^{-1} at 20-30 °C and CH_4, ~ 1.2-1.4 mol kg^{-1} at 30 °C [51,53,54]. In contrast, there is a lack of data for the adsorbed concentration of Ar on this material.

The adsorption isotherms confirm that 5A zeolite is a suitable adsorbent for hydrogen purification due to its low H_2 adsorption capacity compared with the values obtained for the other gases (N_2, CH_4, and Ar). The parameters of the DSL model are summarized in Table 6. The adsorption heat of the studied gases follows the same trend as the adsorption capacities described above, and these parameters are in accordance with those reported for N_2 and CH_4 on zeolite 5A elsewhere [51,53].

Table 6. Dual-site Langmuir parameters on 5A zeolite

Parameter	Units	H_2	N_2	CH_4	Ar
$q_{\max,1}$	mol kg ^{1}	2.58	2.37	2.79	1.69
$b_{\infty,1}$	bar^{-1}	$2.01\cdot10^{-4}$	$3.60\cdot10^{-5}$	$1.91\cdot10^{-5}$	$1.63\cdot10^{-4}$
$\Delta H_1 = \Delta H_2$	kJ mol^{-1}	9.45	20.88	23.13	13.88
$q_{\max,2}$	mol kg^{-1}	0.39	0.95	1.76	5.0
$b_{\infty,2}$	bar^{-1}	$3.12\cdot10^{-5}$	$4.85\cdot10^{-5}$	$1.90\cdot10^{-5}$	$6.99\cdot10^{-5}$
RSS	%	$5.64\cdot10^{-5}$	$1.98\cdot10^{-3}$	$2.48\cdot10^{-2}$	$6.10\cdot10^{-5}$

3.2. Mono- and multicomponent breakthrough tests

Breakthrough experiments are required to study the adsorption bed dynamics and to validate the mathematical model. Accordingly, breakthrough curves were measured at different operational conditions of feed flowrate and pressure according to Table 3. The results of the single component adsorption and desorption breakthroughs of H_2, Ar, N_2 and CH_4 on 5A zeolite are illustrated in Figure 6. The reversibility of single and multicomponent breakthroughs was confirmed as the adsorption and desorption values fall on the same trend line. The breakthrough times of single component for H_2, Ar, N_2 and CH_4 are approximately 31 s, 80 s, 190 s and 270 s, respectively, at 1 bar and 0.5 L_N min^{-1}, whereas the values change to 29 s, 70 s, 130 s and 200 s, respectively, at 4.5 bar and 2.75 L_N min^{-1}. This indicates that the first impurity to break through the column is Ar, followed by N_2 and CH_4. The results show that Ar adsorbs only slightly and H_2 adsorbs significantly less than Ar. However, the fast breakthrough of Ar on zeolite 5A may negatively affect H_2 purity and recovery. Therefore, H_2 product of the PSA unit packed with zeolite 5A is expected to be controlled by the concentration of Ar.

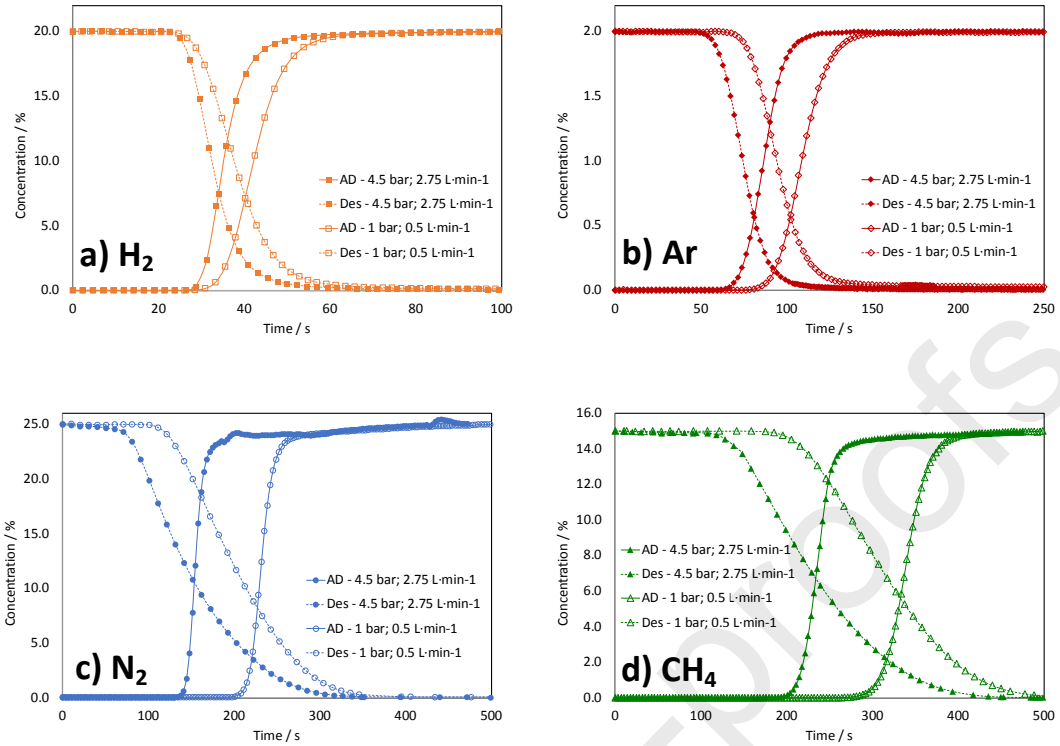

Figure 6. Single component adsorption and desorption breakthroughs of a) H_2, b) Ar, c) N_2 and d) CH_4 on 5A zeolite. Solid lines, adsorption; dashed line, desorption.

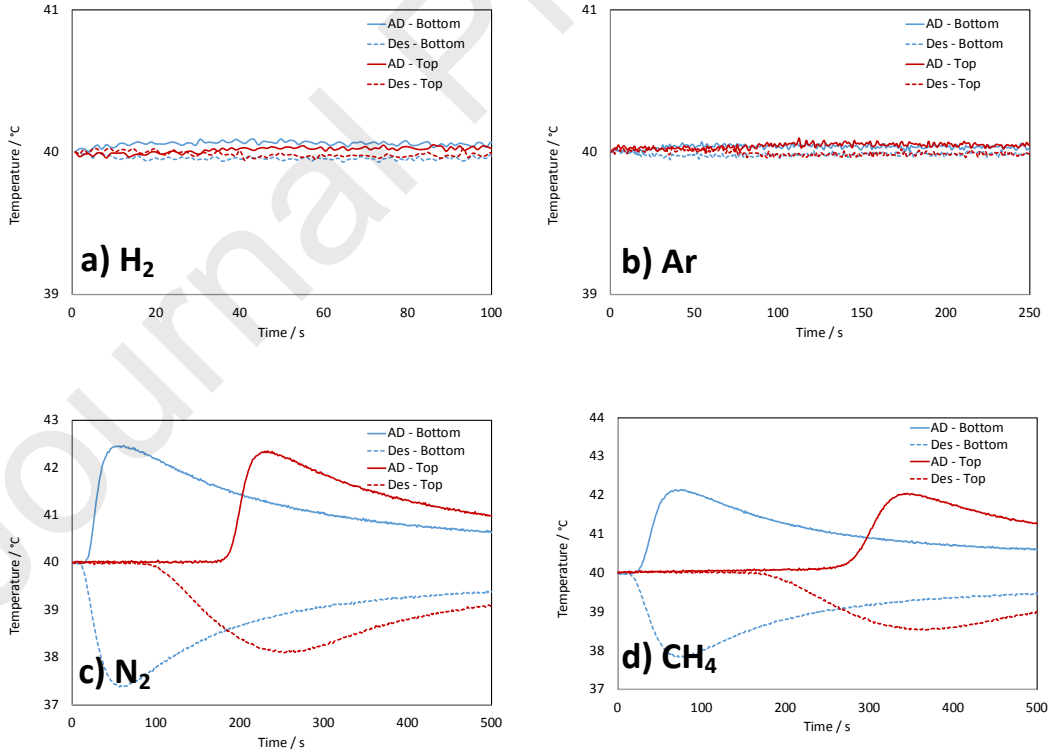

Figure 7. Temperature history of the single component breakthroughs of a) H_2, b) Ar, c) N_2 and d) CH_4, at 0.5 L_N min^{-1}, 1bar and 40 °C. Solid lines, adsorption; dashed line, desorption.

Moreover, Figure 7 reports the inner-temperature profiles at the bottom and the top of the column for the breakthrough curves depicted in Figure 6. Due to the low amount of H_2 and Ar adsorbed, the temperature peaks corresponding to these components were negligible. Likewise, the temperature remains nearly constant for Ar and H_2 desorption breakthroughs, while a temperature decrease is observed for N_2 and CH_4.

The comparison of the simulation results with the experimental single component and multicomponent data at 0.5 L_N min^{-1}, 1 bar and 40 °C, is included in Figure 8 and Figure 9, respectively. Despite the simplifications, the dynamic mathematical model is in reasonable agreement with the experimental breakthrough curves for the concentration and temperature. The breakthrough curves are predicted with a slight advanced breakthrough time and temperature not exceeding 20 s and 1 °C, respectively. Furthermore, as depicted in Figure 9, the breakthrough times for H_2, Ar, N_2 and CH_4 from multicomponent mixtures are very similar to the values given above for single component breakthroughs.

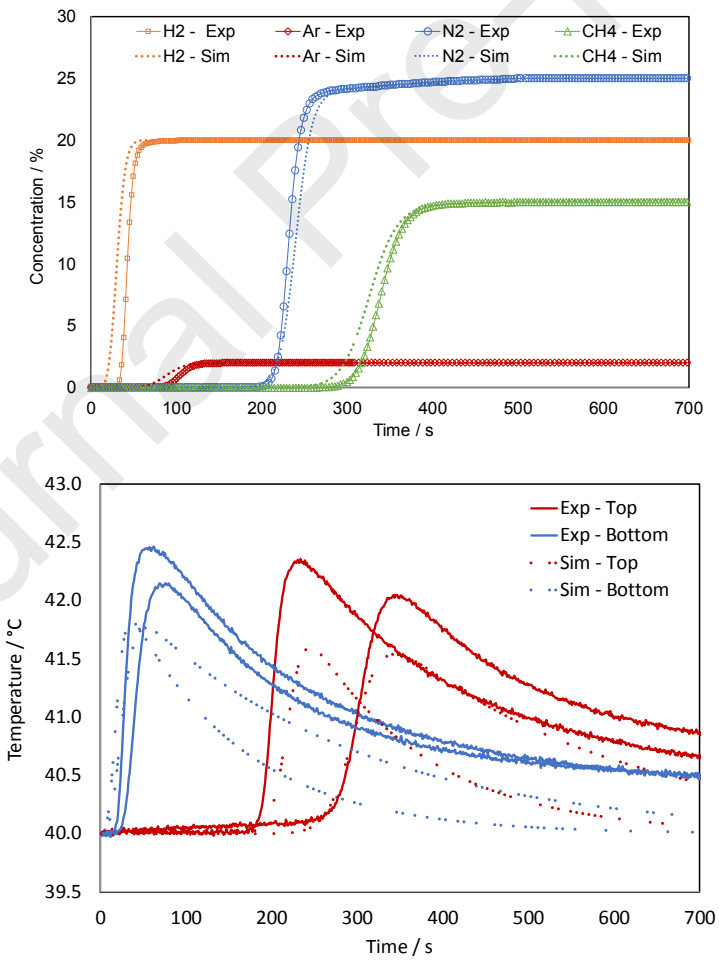

Figure 8. Comparison between the simulation and the experimental single component breakthrough data, at 0.5 L_N min^{-1}, 1bar and 40 °C. Solid lines denote the experimental data; dotted lines denote the simulated data.

Regarding the temperature effect, the temperate history at the bed inlet (T – Bottom) displays only one peak corresponding to all components of the mixture, since the different components have not been separated yet. In turn, at the top of the column (T – Top), the two peaks of temperature, at *ca*. 42.3 °C, at instants 190 s and 270 s correspond to the adsorption heat generated by the concentration fronts of adsorbates N_2 and CH_4, respectively.

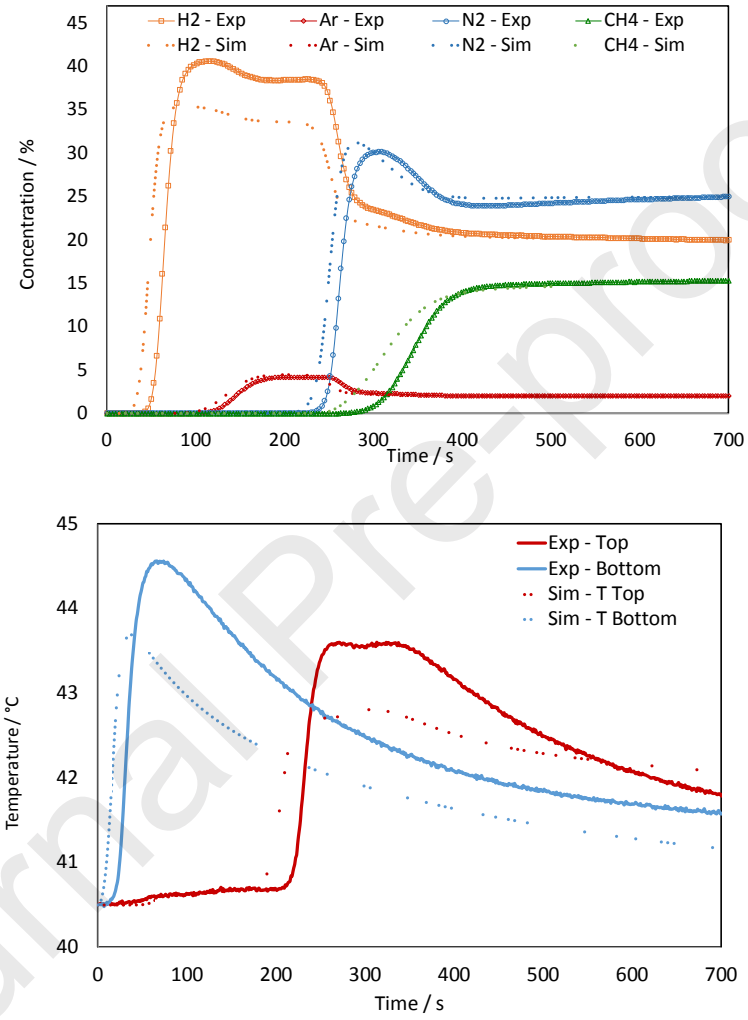

Figure 9. Comparison between the simulation and the experimental multicomponent breakthrough data, at 0.5 L_N min^{-1}, 1bar and 40 °C. Solid lines denote the experimental data; dotted lines denote the simulated data.

3.3. PSA experiments

A set of PSA experiments were performed as indicated in Table 4. To reach the cyclic steady-state, the four-bed PSA unit was operated experimentally for at least 40 cycles, until the product concentration history remained constant. Table 7 summarizes a total of 24 PSA tests performed, including the experimental results obtained for each run as well as the modeled results. Runs #1 to #16 were designed based on CCD methodology,

while runs #17 to #24 were undertaken as screening experiments and replicates for assessing the experimental reproducibility. The results show that CH_4 concentrations were below the detection limit of the gas analyzer, except for run #21 at P/F = 0.04.

Table 7. Performance of the cyclic PSA unit

	DoE factors			Experimental process responses					RSM predictions	
run nº	P_h (bar)	t_{AD} (s)	P/F (-)	HP (%vol.)	y_{N2+Ar} (ppm)	y_{CH_4} (ppm)	HR (%)	Productivity (mol_{H_2}/kg·day)	HP (%vol.)	HR (%)
1	7	90	0.11	99.51	4940	<100	71.4	391.6	99.52	71.9
2	8	75	0.20	99.99	<100	<100	43.3	237.7	100.0	43.6
3	8	75	0.21	+99.98	<100	<100	43.2	237.1	100.0	43.1
4	9	75	0.20	+99.98	<100	<100	37.2	203.8	99.99	36.7
5	8	60	0.23	+99.98	<100	<100	28.1	154.2	99.99	28.5
6	7	60	0.15	99.98	183	<100	49.4	271.0	99.99	49.4
7	8	75	0.14	+99.98	<100	<100	50.9	279.2	99.99	51.4
8	8	75	0.14	+99.98	<100	<100	50.3	275.8	99.99	50.8
9	8	75	0.09	99.84	1551	<100	62.1	340.7	99.85	60.8
10	9	90	0.09	99.89	1111	<100	61.6	337.1	99.87	61.7
11	9	90	0.10	99.88	1170	<100	60.7	333.4	99.90	59.7
12	7	60	0.09	99.82	1764	<100	60.6	334.0	99.81	61.0
13	8	90	0.18	99.92	752	<100	56.2	308.1	99.90	56.3
14	7	75	0.19	99.96	447	<100	54.9	301.4	99.94	54.2
15	9	60	0.13	+99.98	<100	<100	37.4	205.3	100.0	36.7
16	9	60	0.16	+99.98	<100	<100	29.7	162.7	100.0	30.7
17	9	90	0.16	99.97	325	<100	40.0	219.6	99.99	51.5
18	7	90	0.09	99.12	8820	<100	75.4	413.6	99.41	75.1
19	9	75	0.10	99.99	<100	<100	52.5	283.1	99.97	53.4
20	9	75	0.08	99.93	740	<100	55.9	306.6	99.94	56.6
21	8	90	0.04	98.27	16043	1272.12	79.5	436.0	99.41	77.4
22	8	75	0.06	99.49	5090	<100	68.1	373.5	99.71	68.0
23	9	60	0.17	+99.98	<100	<100	30.9	170.0	100.0	30.0
24	9	90	0.16	99.98	245	<100	51.4	282.0	99.99	51.9

Two empirical models, previously described by Eq. (10), were fitted for H_2 purity and recovery, from the CCD results, using the statistical software JMP. Model parameters of model 1 for describing hydrogen purity, HP, and model 2 for describing hydrogen recovery, HR, as well as the statistical and regression parameters are presented in Table 8. All parameters display a p-value smaller than 5 %; moreover, the empirical models describe accurately the experimental results with determination coefficients of R^2 = 0.985 and R^2 = 0.997, for HP and HR, respectively.

Table 8. ANOVA for response surface models

	Model 1, HP		Model 2, HR	
Parameter	**Estimate**	**p-value**	**Estimate**	**p-value**
β_0	99.99	<.0001	51.5	<.0001
β_1	-0.10	<.0001	9.2	<.0001
β_2	0.10	<.0001	-7.5	<.0001
β_3	0.19	<.0001	-17.5	<.0001
β_4	0.08	<.0001	0.3	0.464
β_5	0.07	0.014	4.1	0.003
β_6	-0.13	<.0001	-1.3	0.189

β_7	-0.04	0.004	-0.7	0.198
β_8	-0.05	0.001	1.4	0.024
β_9	-0.24	<.0001	6.4	0.005
R^2	0.985		0.997	
RMSE	0.02		0.92	
p-value	<0.0001		<0.0001	

3.3.1. The effect of independent factors on responses

The response surfaces of these models are displayed in Figure 10, for adsorption pressures at 7 bar (green), 8 bar (blue) and 9 bar (red). This figure shows similar surface shapes for the three pressures. As it can be seen, an increase in adsorption pressure leads to a purity increase (Fig. 10 (a)) whereas the recovery (Fig. 10 (b)) and productivity drop. The same trend is observed increasing the P/F ratio while the opposite trend is observed increasing the t_{ad}. The maximum product purity occurs at the P/F ratio upper bound because P/F enhances the adsorbent regeneration. However, the recovery and productivity decreases, as P/F ratio increased, due to higher amount of H_2 used in the purge step. An optimal value of t_{ad} should allow enough time for H_2 concentration front to leave the adsorption bed, and it should be short enough to avoid the impurities front to breakthrough.

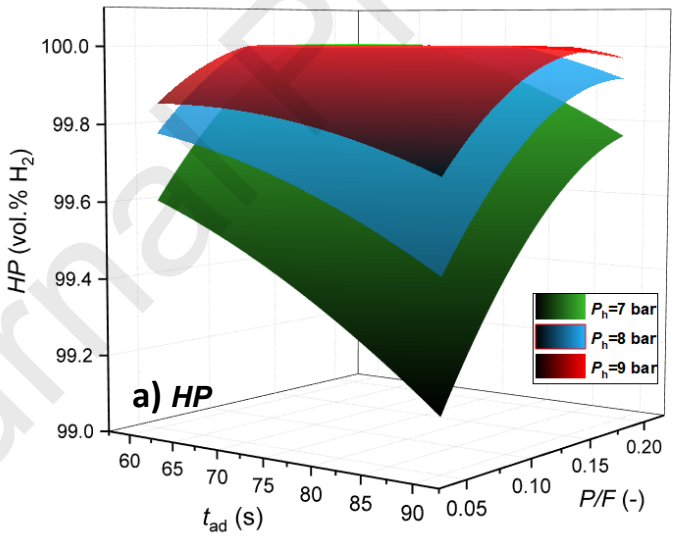

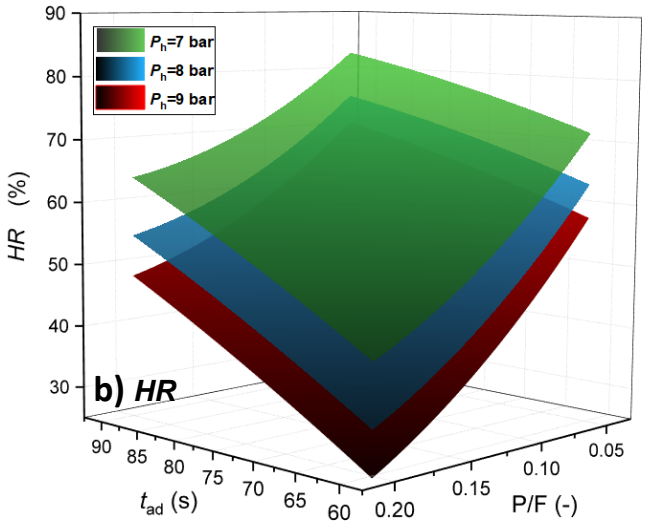

Figure 10. Response surface for hydrogen purity $\boldsymbol{HP}$ and recovery $\boldsymbol{HR}$, as a function of the independent variables $\boldsymbol{t_{ad}}$ and $\boldsymbol{P/F}$ ratio at 7 bar (green); 8 bar (blue); and 9 bar (red).

3.3.2. Process optimization

The four-column PSA system was optimized for delivering three different hydrogen qualities: high purity for PEMFC road vehicle systems (Type I, Grade D), medium purity for PEMFC stationary appliance systems (Type I, Grade E) and lower purity for industrial use to feed conventional ICE (Type I, Grade A), in compliance with ISO 14687 standards [9–11]. The optimization was performed maximizing the recovery for each H_2 quality using the desirability function of JMP software application, as follows:

- Opt #1, maximizes the recovery and sets the H_2 purity to 99.97 %vol.
- Opt #2, maximizes the recovery and sets the H_2 purity to 99.9 %vol.
- Opt #3, maximizes the recovery and sets the H_2 purity to 98.0 %vol.

Then, additional experiments were performed under the optimal conditions predicted by the model. The obtained experimental and model results can be found in Table 9. As it can be seen, the RSM predicted optimum performance parameters very close to the experimental values. For obtaining PEMFC mobility grade H_2 at 99.97 % (Opt #1), a recovery of 55.5 % was obtained experimentally, while the model predicted 54.8 % for P_h = 9 bar; P/F = 0.1; t_{ad} =84 s, corresponding to a productivity of 304 mol_{H2} $kg_{ads}^{-1}day^{-1}$ and 282 ppm of Ar. Setting the H_2 concentration to 99.9 %vol. (Opt #2), the forecasted optimum operating conditions were P_h= 9 bar; P/F = 0.08; t_{ad} = 83 s. For these operating conditions the experimental recovery was 61.0 % while the forecasted is 60.3; the productivity was 335 mol_{H2} kg_{ads}^{-1} day^{-1} and 831 ppm of Ar. Setting H_2 concentration to

98 %vol. (Opt #3), for P_h= 7 bar; P/F = 0.09; t_{ad} = 90 s, an experimental and model recoveries of 75.3 % and 75.6 %, respectively, were obtained, corresponding to a productivity of 413 mol_{H2} $kg_{ads}^{-1}day^{-1}$ and 7514 ppm of inerts.

Additionally, the experimental run Opt #2.1 was performed but with a feed stream free of Ar (H_2:N_2:CH_4; 60:25:15 vol.%). This allowed to evaluate the contribution of Ar to the inert content at the product stream, since Ar and N_2 were quantified as one. An experimental recovery of 99.98 % was obtained, which indicates that the inert gases concentration at the product stream was mostly Ar.

Table 9. Optimal DoE parameters and experimental and RSM predicted PSA results

	DoE factors			Experimental process responses					RSM pred.	
run nº	P_h (bar)	t_{AD} (s)	*P/F* (-)	HP (%vol.)	y_{N_2+Ar} * (ppm)	y_{CH_4} (ppm)	HR (%)	*Productivity* (mol_{H2}/kg·day)	HP (%vol.)	HR (%)
Opt #1	9	84	0.11	99.97	281	<100	55.50	304.4	99.97	54.8
Opt #2	9	83	0.08	99.92	831	<100	61.02	334.8	99.90	60.3
Opt #2.1	9	83	0.08	+99.98	<100	<100	61.02	334.8	-	-
Opt #3	7	90	0.09	99.25	7514	<100	75.30	413.1	99.11	75.6

* The optimization Opt#2.1 indicates that the inert content (N_2+Ar) observed for Opt #2 is mostly Ar.

3.4. Economic benefits

The use of surplus hydrogen from industrial processes provides a cheaper H_2 source that can be used as a transportation fuel for road vehicle applications. The cost of H_2 produced from waste streams of ammonia plants, using a small-PSA unit, was estimated and compared to the conventional SMR pathway as the most cost-effective option. The comparison also considers the compression of the purified hydrogen to 350 and 700-bar and its delivery to the nearest retail HRS. Furthermore, the levelized cost of H_2 should include the annualized capital costs (CAPEX) of the PSA unit and compressors as well as the operating costs (OPEX), due to electric energy consumption along with distribution costs in the off-site option. The detailed equations used to assess the process economics are outlined in Appendix C.

Up to 10 % of the hydrogen consumed by relevant industries, including ammonia plants, is burnt away in flare stacks, or is directly emitted to the atmosphere [29]. In a small-to-medium ammonia production plant of 500 ton of NH_3 day^{-1}, a stream of up to 12.5 kg_{H2} h^{-1} (at 99.97 %vol. H_2 and *ca.* 20 bar) can be produced on-site via PSA technology of the purge gases of the ammonia synthesis process [33,37]. This hydrogen quantity was estimated based on the recovery of 55.0 % achieved in the present work.

The cost of producing fuel cell grade H_2 *in situ* from purge gases of ammonia plants using small-PSA units is estimated to be 0.63 € kg H_2^{-1}, which is similar to the cost of purifying H_2 by SMR. However, when considering off-site conventional SMR plants, H_2 production costs are currently estimated to be around 2 € kg H_2^{-1} and strongly depend on the price of natural gas. In this regard, the recovered hydrogen from APG can be sold directly at the factory site as a chemical commodity with competitive prices or as H_2 fuel for FCEVs, whose market is steadily increasing. In such a scenario, compressed gas cylinders are a good alternative for low demands and short distance delivering [55,56]. The produced H_2 should be compressed from *ca.* 20 bar to 350/700 bar, according to the different current pressure levels of the tank systems between buses/trucks (350 bar) and passenger cars (700 bar) [5]. Lastly, compressed hydrogen (CH2) can be transported by tube trailers to the nearest available HRS (<20 km) [57]. The techno-economic assessment is summarized in Table 10 and discussed below.

Table 10. Cost sheet of hydrogen recovery via small-scale PSA

	H_2 at 20 bar	**H_2 at 350 bar**	**H_2 at 700 bar**
CAPEX (€)			
PSA unit	321,000	321,000	321,000
Compressor (s)	-	179,600	241,600
Sub-total	321,000	500,600	562,600
OPEX (€/year)			
PSA unit	28,700	28,700	28,700
Compressor (s)	-	24,800	31,600
CH2 delivery	-	22,000	22,000
Sub-total	28,700	75,500	82,300
Levelized cost (€/kg H_2)	**0.63**	**1.17**	**1.39**

Based on the economic assumptions described above, the cost to purify ammonia waste H_2 hydrogen stream using small-PSA units, compress and transport is ca. 1.17 and 1.39 € kg H_2^{-1}, respectively, depending on the dispensing pressure of 350 or 700 bar. These values permit reducing H_2 costs by at least 40 %; this saving value was calculated based on off-site H_2 production by SMR plus compression and transportation until the refueling station [58]. Although the economic assumptions may vary both with time and location, the resultant costs are reasonable values as they entail the essential stages of the waste-to-hydrogen production route. As a distributed hydrogen production, these hydrogen sources can be crucial in the early stage of transition to the future global hydrogen-incorporated economy, pushing hydrogen down to competitive prices. These estimations strongly depend on the available volume of the waste hydrogen streams.

4. CONCLUSIONS

Industrial hydrogen-rich waste streams hold promise in their upgrading to feed fuel cell stacks. As in the ammonia synthesis process, a gaseous stream is purged to keep the inert gases concentration below a threshold value, this stream contains large hydrogen quantities, which can be recovered. A four-bed PSA unit packed with 5A zeolite was studied to purify hydrogen from a simulated effluent gas (H_2:N_2:CH_4:Ar, 58:25:15:2 %) of ammonia synthesis process.

The adsorption equilibrium isotherms of H_2, N_2, CH_4, and Ar on four pre-selected adsorbents was obtained. According to the equilibrium separation factor it was concluded that activated carbon AC is the best adsorbent for removing Ar, whereas LiX and 5A zeolites remove more effectively N_2 and CH_4, respectively. Therefore, 5A zeolite was selected as the best adsorbent for purifying H_2 from ammonia purge gas stream due to its well-balanced N_2/H_2 and CH_4/H_2 separation factors and acceptable Ar removal performance.

To assess the performance of the selected adsorbent, 5A zeolite, single component and multicomponent breakthrough curves were experimentally carried out in a single packed column, and further simulated. The results, simulations and experimental, indicate that the first impurity to break thought the column is Ar, followed by N_2 and finally by CH_4. Consequently, the separation performance of the four-bed PSA unit packed with zeolite 5A can be affected by the Ar adsorption for concentrations as low as 2 %.

The PSA experiments were conducted in a 4-column PSA unit with 12-events cycle, comprising 9 elementary steps. The role of operating parameters in PSA performance such as *P/F* ratio, adsorption step time and adsorption pressure, was investigated. The overall PSA performance was evaluated in terms of purity, recovery and productivity of H_2 product. The experimental unit was optimized to maximize the responses based on RSM models for three specific final applications, in compliance with ISO 14687 standards. The PSA unit of this study could produce H_2 with 99.25 - 99.97% purity with 55.5 – 75.3 % of recovery, respectively, where Ar and N_2 were the main impurities at the product stream. A significant loss of recovery and productivity happens when H_2 purity was set at +99.9 %vol. The study showed the feasibility of the PSA process packed with 5A zeolite to produce a wide purity range of H_2 product streams from a feed mixture containing as impurities N_2, CH_4 and Ar, as simulated ammonia purge gas.

In addition to the technical performance, a simplified economic analysis has been carried out. The cost to purify an ammonia waste hydrogen stream to +99.97 % using a small-

PSA unit, compress and transport has been estimated to be 1.17 to 1.39 € kg H_2^{-1}, respectively, depending on the dispensing pressure of 350 or 700 bar; these values were estimated to be 40 % below the current commercial costs.

ACKNOWLEDGMENTS

This research was supported by the projects CTQ2015-66078-R (MINECO/FEDER) and SOE1/P1/E0293 (INTERREG SUDOE /FEDER, UE), "Energy Sustainability at the Sudoe Region: Red PEMFC-Sudoe". Adélio Mendes and Frederico Relvas acknowledge to projects UID/EQU/00511/2019 funded by national funds through FCT/MCTES (PIDDAC); and "LEPABE-2-ECO-INNOVATION" – NORTE-01-0145-FEDER-000005, funded by Norte Portugal Regional Operational Programme (NORTE 2020), under PORTUGAL 2020 Partnership Agreement, through the European Regional Development Fund (ERDF). Frederico Relvas also acknowledges NORTE-08-5369-FSE-000028 supported by NORTE 2020, under the Portugal 2020 Partnership Agreement and the European Social Fund (ESF).

APPENDIX. SUPLEMENTARY DATA

APPENDIX A: Equilibrium adsorption isotherms

APPENDIX B: Simulation approach of breakthrough curves

APPENDIX C: Economics

NOMENCLATURE

Parameters

L_{bed} length of the column (cm)

P_{i}, P_{j} partial pressure in the gas phase (bar)

R^2 determination coefficient (-)

X_{i} dimensionless process factors

b_{∞} affinity constant at infinite temperature (bar^{-1})

d_{p} particle diameter (mm)

k_{i} mass transfer coefficient (s^{-1})

m_{ads} adsorbent mass loaded to the bed (kg)

q^* molar concentration in the adsorbed phase (mol kg^{-1})

q_{max} isotherm parameter, maximum adsorbed concentration (mol kg^{-1})

t_{cycle} total operating time during an entire cycle (s)

$\alpha_{i/j}$ separation factor between gases *i* and *j* (-)

$\hat{y}$ process response (-)

HP hydrogen purity (%)

HR hydrogen recovery (%)

P pressure (bar)

P/F purge-to-feed ratio (-)

Q volumetric flow rate (L_N min^{-1})

R ideal gas constant (J mol^{-1} K^{-1})

$RMSE$ root-mean-square-error (-)

RSS residual sum of squares (%)

T temperature (°C)

b affinity constant (bar^{-1})

d diameter (cm)

t time variable (s)

y gas-phase mole fraction (-)

Greek symbols

ρ_p particle density (g cm^{-3})

ΔH heat of adsorption (J mol^{-1})

β polynomial model coefficient (-)

Abbreviations

AD adsorption

AD/BF providing backfill

ANOVA analysis of variance

APG ammonia purge gas

BD blowdown

BF backfill

BPR backpressure regulator

CAPEX capital costs

CCD central composite design

CCS carbon capture and storage

CH2 compressed hydrogen

DoE design of experiments

DPE depressurization pressure equalization

DSL dual site Langmuir model

EU	European Union
FCEV	fuel cell electric vehicles
FPPE	first pressurization pressure equalization
GHG	greenhouse-gas
HRS	hydrogen refueling station
ICE	internal combustion engine
ICE	internal combustion engine
ISO	International Standard Organization
LDF	linear driving force model
MFC	flow controller
MFM	flow meter
ODE	ordinary differential equation
OPEX	operating costs
PDE	partial differential equation
PEMFC	polymer electrolyte membrane fuel cells
PG	purge
PSA	pressure swing adsorption
RSM	response surface methodology
SMR	steam methane reforming
SPPE	second pressurization pressure equalization
TCD	thermal conductivity detector
TT	thermocouple
UDS	upwind differencing scheme

Subscripts

+1	upper level of the DoE factor
0	outside
-1	lower level of the DoE factor
1, 2	dual-site Langmuir sites
ad	adsorption
eq	equalization
exp	experimental data
F	feed stream
h	high
i, j	gas component
in	inside
k	experimental adsorption data point

l	low
mod	modeling data
N	total number of experimental adsorption data points
prod	product

REFERENCES

[1] IRENA International Renewable Energy Agency, Global Energy Transformation: A Roadmap to 2050, 2018. www.irena.org.

[2] International Energy Agency (IEA), Summary: Energy Technology Perspectives 2017, OECD/IEA. (2017). www.iea.org.

[3] FCH JU, Hydrogen Roadmap Europe: A sustainable pathway for the European Energy Transition, 2019.

[4] Hydrogen Europe's Strategic Plan 2020-2030, Hydrogen: enabling a zero emission Europe, 2018.

[5] R.B. GmbH, Fuel Cell Electric Buses - Potential for Sustainable Public. Transport in Europe, FCH JU., 2015.

[6] FCH-JU Study, Study on early business cases for H2 in energy storage and more broadly power to H2 applications, 2017.

[7] M. Díaz, A. Ortiz, I. Ortiz, Progress in the use of ionic liquids as electrolyte membranes in fuel cells, J. Memb. Sci. 469 (2014) 379–396. doi:10.1016/j.memsci.2014.06.033.

[8] F. Blank, M. Klages, S. Mock, G. Toth, DAIMLER: The Importance of Fuel Quality, 2017. www.hycora.eu/workshops.

[9] ISO 14687: Hydrogen Fuel : Product Specification, Part 1: All Applications Except Proton Exchange Membrane (PEM) Fuel Cell for Road Vehicles, 2009.

[10] ISO 14687: Hydrogen Fuel : Product Specification, Part 2: Proton exchange membrane (PEM) fuel cell applications for road vehicles, (2009).

[11] ISO 14687: Hydrogen Fuel : Product Specification, Part 3: Proton exchange membrane (PEM) fuel cells applications for stationary appliances, (2009).

[12] M.G. Shalygin, S.M. Abramov, A.I. Netrusov, V. V. Teplyakov, Membrane recovery of hydrogen from gaseous mixtures of biogenic and technogenic origin, Int. J. Hydrogen Energy. 40 (2015) 3438–3451. doi:10.1016/j.ijhydene.2014.12.078.

[13] T. Abbasi, S.A. Abbasi, “Renewable” hydrogen: Prospects and challenges, Renew. Sustain. Energy Rev. 15 (2011) 3034–3040. doi:10.1016/j.rser.2011.02.026.

[14] M. Yáñez, A. Ortiz, B. Brunaud, I.E. Grossmann, I. Ortiz, Contribution of upcycling surplus hydrogen to design a sustainable supply chain: The case study of Northern Spain, Appl. Energy. 231 (2018). doi:10.1016/j.apenergy.2018.09.047.

[15] J.L. Aprea, “Quality specification and safety in hydrogen production, commercialization and utilization,” Int. J. Hydrogen Energy. 39 (2014) 8604–8608. doi:10.1016/j.ijhydene.2014.01.005.

[16] D. Stolten, B. Emonts, Hydrogen Science and Engineering: Materials, Processes, Systems and Technology, Weinheim, Germany, 2016.

[17] J.A. Delgado, M.A. Uguina, J.L. Sotelo, B. Ruíz, J.M. Gómez, Fixed-bed adsorption of carbon dioxide/methane mixtures on silicalite pellets, Adsorption. 12 (2006) 5–18. doi:10.1007/s10450-006-0134-3.

[18] Shivaji Sircar and Timothy C. Golden, Pressure Swing Adsorption Technology for Hydrogen Production, in: Hydrog. Syngas Prod. Purif. Technol., John Wiley & Sons, Inc., Hoboken, New Jersey, 2009: pp. 414–450.

[19] U. Itsuki, Separation and purification of hydrogen, in: Energy Carriers Convers. Syst. Vol. 2., Encyclopedia of Life Support Systems (EOLSS), 2009: pp. 268–282.

[20] M.D. LeVan, Pressure Swing Adsorption: Equilibrium Theory for Purification and Enrichment, Ind. Eng. Chem. Res. 34 (1995) 2655–2660. doi:10.1021/ie00047a014.

[21] F.V.S. Lopes, C.A. Grande, A.E. Rodrigues, Activated carbon for hydrogen purification by pressure swing adsorption: Multicomponent breakthrough curves and PSA performance, Chem. Eng. Sci. 66 (2011) 303–317. doi:10.1016/j.ces.2010.10.034.

[22] A. Malek, S. Farooq, Hydrogen purification from refinery fuel gas by pressure swing adsorption, AIChE J. 44 (1998) 1985–1992. doi:10.1002/aic.690440906.

[23] J. Yang, C.-H. Lee, Adsorption dynamics of a layered bed PSA for H2 recovery from coke oven gas, AIChE J. 44 (1998).

[24] H. Ahn, J. Yang, C.H. Lee, Effects of feed composition of coke oven gas on a layered bed H2 PSA process, Adsorption. 7 (2001) 339–356. doi:10.1023/A:1013138221227.

[25] S. Ahn, Y.W. You, D.G. Lee, K.H. Kim, M. Oh, C.H. Lee, Layered two- and four-bed PSA processes for H2 recovery from coal gas, Chem. Eng. Sci. 68 (2012) 413–423. doi:10.1016/j.ces.2011.09.053.

[26] Foundation for Research and Technology Hellas, Final Report Summary - HY2SEPS-2 project (Hybrid Membrane- Pressure Swing Adsorption (PSA) Hydrogen Purification Systems), 2015.

[27] R.L. Schendel, C.L. Mariz, J.Y. Mak, Is permeation competitive?, Hydrocarb. Process. 62 (1983).

[28] Environmental assessment (EA/ HU / 029) - Fertiberia, S.A. in Palos de la Frontera (Huelva), 2007.

[29] S.C.T. J. Perrin, R. Steinberger-Wilkens, CertifHy project “Designing the 1st EU-wide Green and Low Carbon Certification System,” 2007.

[30] S. Favreau, D., & Vinot, Roads2HyCom Project: Fuel cells and hydrogen in a sustainable energy economy, (2009).

[31] S.-H. Cho, K.-T. Chue, J.-N. Kim, A two stage PSA for argon and hydrogen recovery from ammonia purge gas, Chem. Eng. Commun. 163 (1998).

[32] M.R. Rahimpour, A. Asgari, Modeling and simulation of ammonia removal from purge gases of ammonia plants using a catalytic Pd–Ag membrane reactor, J. Hazard. Mater. 153 (2008) 557–565. doi:10.1016/j.jhazmat.2007.08.095.

[33] M.R. Rahimpour, A. Asgari, Production of hydrogen from purge gases of ammonia plants in a catalytic hydrogen-permselective membrane reactor, Int. J. Hydrogen Energy. 34 (2009) 5795–5802. doi:10.1016/j.ijhydene.2009.05.013.

[34] F. Siavashi, M. Saidi, M.R. Rahimpour, Purge gas recovery of ammonia synthesis plant by integrated configuration of catalytic hydrogen-permselective membrane reactor and solid oxide fuel cell as a novel technology, J. Power Sources. 267 (2014). doi:10.1016/j.jpowsour.2014.05.072.

[35] T. Dong, L. Wang, A. Liu, X. Guo, Q. Ma, G. Li, Q. Sun, Experimental study of separation of ammonia synthesis vent gas by hydrate formation, Pet. Sci. 6 (2009). doi:10.1007/s12182-009-0030-z.

[36] Fertilizer company personal communication, (2017).

[37] Z. Wu, W. Wenchuan, The recovery of ammonia from purge gas, (n.d.). http://www.cryobridge.com/Ammonia.pdf.

[38] J.C. Santos, F.D. Magalhães, A. Mendes, Contamination of zeolites used in

oxygen production by PSA: Effects of water and carbon dioxide, Ind. Eng. Chem. Res. 47 (2008) 6197–6203. doi:10.1021/ie800024c.

[39] D.K. Moon, D.G. Lee, C.H. Lee, H2 pressure swing adsorption for high pressure syngas from an integrated gasification combined cycle with a carbon capture process, Appl. Energy. 183 (2016) 760–774. doi:10.1016/j.apenergy.2016.09.038.

[40] R.T. Yang, Sorbents for Applications, in: Adsorbents Fundam. Appl., Wiley-Interscience, 2003: pp. 280–381.

[41] D. Broom, Characterizing adsorbents for gas separations, Chem. Eng. Prog. 114 (2018) 30–37.

[42] M. Bastos-Neto, A. Moeller, R. Staudt, J. Böhm, R. Gläser, Dynamic bed measurements of CO adsorption on microporous adsorbents at high pressures for hydrogen purification processes, Sep. Purif. Technol. 77 (2011) 251–260. doi:10.1016/j.seppur.2010.12.015.

[43] D. Ferreira, R. Magalhães, P. Taveira, A. Mendes, Effective adsorption equilibrium isotherms and breakthroughs of water vapor and carbon dioxide on different adsorbents, Ind. Eng. Chem. Res. 50 (2011) 10201–10210. doi:10.1021/ie2005302.

[44] A.M. Ribeiro, C.A. Grande, F.V.S. Lopes, J.M. Loureiro, A.E. Rodrigues, A parametric study of layered bed PSA for hydrogen purification, Chem. Eng. Sci. 63 (2008) 5258–5273. doi:10.1016/j.ces.2008.07.017.

[45] F. Relvas, R.D. Whitley, C. Silva, A. Mendes, Single-Stage Pressure Swing Adsorption for Producing Fuel Cell Grade Hydrogen, Ind. Eng. Chem. Res. 57 (2018) 5106–5118. doi:10.1021/acs.iecr.7b05410.

[46] C.A. Grande, Advances in Pressure Swing Adsorption for Gas Separation, ISRN Chem. Eng. 2012 (2012) 1–13. doi:10.5402/2012/982934.

[47] P. Cruz, J.C. Santos, F.D. Magalhaes, A. Mendes, Cyclic adsorption separation processes: Analysis strategy and optimization procedure, Chem. Eng. Sci. (2003). doi:10.1016/S0009-2509(03)00189-1.

[48] J.K. Telford, A brief introduction to design of experiments, Johns Hopkins APL Tech. Dig. (Applied Phys. Lab. 27 (2007) 224–232.

[49] M.J. Anderson, P.J. Whitcomb, RSM Simplified: Optimizing Processes Using Response Surface Methods for Design of Experiments, CRC Press Book, 2017.

[50] Ž.R. Lazić, Design of Experiments in Chemical Engineering, Wiley-VCH: Weinhem, Weinheim, Germany, 2005.

[51] G.-M. Nam, B.-M. Jeong, S.-H. Kang, B.-K. Lee, D.-K. Choi, Equilibrium isotherms of CH4, C2H6, C2H4, N2, and H2 on Zeolite 5A using a static volumetic method, J. Chem. Eng. Data. 50 (2005) 72–76.

[52] M. Yavary, H. Ale Ebrahim, C. Falamaki, Competitive Adsorption Equilibrium Isotherms of CO, CO2, CH4, and H2 on Activated Carbon and Zeolite 5A for Hydrogen Purification, J. Chem. Eng. Data. 61 (2016) 3420–3427. doi:10.1021/acs.jced.6b00312.

[53] D.A. Kennedy, M. Mujcin, E. Trudeau, F.H. Tezel, Pure and Binary Adsorption Equilibria of Methane and Nitrogen on Activated Carbons, Desiccants, and Zeolites at Different Pressures, J. Chem. Eng. Data. 61 (2016) 3163–3176. doi:10.1021/acs.jced.6b00245.

[54] J.A.C. Silva, A. Ferreira, P.A.P. Mendes, A.F. Cunha, K. Gleichmann, A.E. Rodrigues, Adsorption Equilibrium and Dynamics of Fixed Bed Adsorption of CH4/N2 in Binderless Beads of 5A Zeolite, Ind. Eng. Chem. Res. 54 (2015) 6390–6399. doi:10.1021/acs.iecr.5b01608.

[55] S. De-León Almaraz, C. Azzaro-Pantel, L. Montastruc, S. Domenech, Hydrogen supply chain optimization for deployment scenarios in the Midi-Pyrénées region, France, Int. J. Hydrogen Energy. 39 (2014) 11831–11845. doi:10.1016/j.ijhydene.2014.05.165.

[56] C. Yang, J. Ogden, Determining the lowest-cost hydrogen delivery mode, Int. J. Hydrogen Energy. 32 (2007) 268–286. doi:10.1016/j.ijhydene.2006.05.009.

[57] J.-H. Han, J.-H. Ryu, I.-B. Lee, Modeling the operation of hydrogen supply networks considering facility location, Int. J. Hydrogen Energy. 37 (2012). doi:10.1016/j.ijhydene.2011.04.001.

[58] International Energy Agency (IEA), Large-Scale Hydrogen Delivery Infrastructure, 2015.

FIGURE CAPTIONS

TABLE CAPTIONS

HIGHLIGHTS

- Upgrading ammonia purge gas to produce different hydrogen qualities
- Characterizing adsorbents for hydrogen purification
- Gas separation performance assessed by breakthrough test and simulations
- Four-column PSA process optimization maximizing hydrogen recovery
- Cost-effective solution to produce low-cost hydrogen as transportation fuel

Declaration of interests

☒ The authors declare that they have no known competing financial interests or personal relationships that could have appeared to influence the work reported in this paper.

☐The authors declare the following financial interests/personal relationships which may be considered as potential competing interests: